The Cryosphere Discuss., 9, 1021–1045, 2015
www.the-cryosphere-discuss.net/9/1021/2015/
doi:10.5194/tcd-9-1021-2015

The Cryosphere Discussions
Open Access

Tomography-based monitoring of isothermal snow metamorphism under advective conditions

P. P. Ebner[1,2], M. Schneebeli[2], and A. Steinfeld[1]

[1]Department of Mechanical and Process Engineering, ETH Zurich, 8092 Zurich, Switzerland
[2]WSL Institute for Snow and Avalanche Research SLF, 7260 Davos-Dorf, Switzerland

Received: 21 January 2015 – Accepted: 4 February 2015 – Published: 18 February 2015

Correspondence to: A. Steinfeld (aldo.steinfeld@ethz.ch) and M. Schneebeli (schneebeli@slf.ch)

Published by Copernicus Publications on behalf of the European Geosciences Union.

Abstract

Time-lapse X-ray micro-tomography was used to investigate the structural dynamics of isothermal snow metamorphism exposed to an advective airflow. Diffusion and advection across the snow pores were analysed in controlled laboratory experiments. The 3-D digital geometry obtained by tomographic scans was used in direct pore-level numerical simulations to determine the effective transport properties. The results showed that isothermal advection with saturated air have no influence on the coarsening rate that is typical for isothermal snow metamorphism. Diffusion originating in the Kelvin effect between snow structures dominates and is the main transport process in isothermal snow packs.

1 Introduction

Snow is a bi-continuous material consisting of fully connected ice and pore space (air) (Löwe et al., 2011). Because of the proximity to the melting point, the high vapour pressure causes a continuous recrystallization of the snow microstructure known as snow metamorphism, even under moderate temperature gradients (Pinzer et al., 2012; Domine et al., 2008). The microstructural changes of snow towards equilibrium under conditions of constant temperature are referred to as isothermal snow metamorphism (Colbeck, 1997a; Kaempfer and Schneebeli, 2007). This is a coarsening process whose driving force is the reduction of the surface free energy of the complex ice–air interface. The energy reduction is achieved by mass transport processes such as vapour diffusion (Neumann et al., 2009), surface diffusion (Kingery, 1960b), volume diffusion (Kuroiwa, 1961), and grain boundary diffusion (Colbeck, 1997a, 1998, 2001; Kaempfer and Schneebeli, 2007). Viscous or plastic flow (Kingery, 1960a), evaporation-condensation with vapour transport (German, 1996; Hobbs and Mason, 1963; Legagneux and Domine, 2005; Maeno and Ebinuma, 1983), and the Kelvin-effect (Bader, 1939; Colbeck, 1980) are also suggested to play an important role. Re-

TCD
9, 1021–1045, 2015

cent studies indicate that vapour transport caused by the Kelvin effect is most important in isothermal metamorphism (Vetter et al., 2010). Snow has a high permeability, which facilitates diffusion of gases and, under appropriate conditions, airflow (Gjessing, 1977; Colbeck, 1989; Sturm and Johnson, 1991; Waddington et al., 1996). Both diffusion and advective airflow affect heat and mass transports in the snow pack (Cunningham and Waddington, 1993; Albert, 1993; McConnell et al., 1998). In the dry snow zone of an ice sheet, Sowers et al. (1992) described a convective zone located just below the surface in which the air is rapidly flushed by convective exchange with the overlying atmosphere. It is suggested that advective flow of air has a direct effect on snow–air exchange processes related to atmospheric chemistry (Clifton et al., 2008; Grannas et al., 2007), and snow metamorphism (Albert and Gilvary, 1992; Albert et al., 2004), and can change the chemical composition of trapped atmospheric gases in ice-cores (Legrand and Mayewski, 1997; Neumann and Waddington, 2004; Severinghaus et al., 2010). However, no prior studies have described the effect of airflow on the vapour transport and the recrystallization of the snow crystals. Over- or undersaturated air leads to a rapid growth or shrinkage of snow structures exposed to such conditions, as exemplified in the growth of surface hoar (Stössel et al., 2010). However, saturation vapour density of the air is reached in the pore space within the first 1 mm of the snow sample, regardless of temperature or flow rate (Neumann et al., 2009; Ebner et al., 2014). The change in shape of the snow crystals during metamorphism also affects the permeability, which, in turn, will continue to affect the shape of the snow structure. Although long-term isothermal metamorphism occurs in nature only in the centre of the polar ice caps (Arnaud et al., 1998), it is important to reduce physical complexity of experiments in order to understand the basic mechanisms governing metamorphism.

The objective of this paper is to study the effect of saturated airflow on the vapour transport and the coarsening rate of snow under isothermal conditions. We designed experiments in a controlled refrigerated laboratory and used time-lapse computed tomography (micro-CT) to obtain the discrete-scale geometry of snow (Schneebeli and Sokratov, 2004; Kaempfer and Schneebeli, 2007; Pinzer and Schneebeli, 2009; Pinzer et al., 2012; Ebner et al., 2014). The extracted 3-D digital geometry of the snow was used to calculate the specific surface area and porosity. Direct pore-level simulations (DPLS) were applied to determine the effective permeability by solving the corresponding mass and momentum conservation equations (Zermatten et al., 2011, 2014).

2 Methodology

Isothermal experiments with fully saturated airflow across snow samples were performed in a micro-CT (Ebner et al., 2014) at laboratory temperatures of $T_{\text{lab}} = -8$ and -15 °C. Figure 1 shows a schematic of the experimental setup. Four different runs were chosen based on the Peclet number ($Pe = u_{\text{D}} d_{\text{p}} / D$ where u_{D} is the superficial velocity in snow, d_{p} is the pore diameter, and D is the diffusion coefficient of water vapour in air) to compare the advective and diffusive transport rates inside the pore space. Experimental runs were performed at 1 atm pressure and volume flow rates of 0 (no advection), 0.36, 3.0, and 5.0 L min^{-1}, corresponding to $Pe = 0$, 0.05, 0.47, and 0.85. Higher Pe numbers were experimentally not possible, as the shear stress by airflow would destroy the snow structure. Natural identical snow was used for the snow sample preparation (water temperature: 30 °C; air temperature: −20 °C) (Schleef et al., 2014). It was sieved with a mesh size of 1.4 mm into two boxes, and sintered for 13 and 27 days at −15 and −5 °C, respectively, for increasing strength and coarsening (Kaempfer and Schneebeli, 2007). A cylinder cut out from the sintered snow was filled into the sample holder. The snow samples were analysed during 96 h with time-lapse micro-CT measurements taken every 8 h, producing a sequence of 13 images. Table 1 summarizes experimental conditions.

The acceleration voltage in the X-ray tube was 70 keV with a nominal resolution of 18 µm. The samples were scanned with 1000 projections per 180°, with an integration time of 200 ms per projection. The innermost 36.9 mm of the total 53 mm diameter were scanned and subsamples with a dimension of 7.2 mm × 7.2 mm × 7.2 mm were extracted for further processing. Absolute z-position varied up to a maximum of 50

TCD
9, 1021–1045, 2015

voxels between subsequent scans due to the weight of the sample holder. To correct for the z-position a linear encoder was built into the micro-CT. A $3 \times 3 \times 3$ median filter and Gaussian filter ($\sigma = 1.4$, support $= 3$) was applied to the reconstructed images. Otsu's method (Otsu, 1979) was used to automatically perform clustering-based image thresholding to segment the grey-level images into ice and air phase. Morphological properties in the two-phase system were determined based on the geometry obtained by the micro-CT. The segmented data were used to calculate a triangulated ice matrix surface and tetrahedrons inscribed into the ice structure. Morphological parameters such as porosity (ε) and specific surface area (SSA) were then calculated. The effective permeability was calculated using the finite volume technique CFD (Computational Fluid Dynamics simulation software from ANSYS) by solving the continuity and Navier–Stokes equations (Zermatten et al., 2011, 2014). A grid convergence study based on the pressure drop (Zermatten et al., 2014) was carried out to find the optimal representative elementary volume (REV) (6.0 mm × 6.0 mm × 3.0 mm). An in-house tetrahedron-based mesh generator (Friess et al., 2013) was used to create the computational grid on the segmented data. The largest mesh element length was 0.153 mm and the smallest possible mesh element measured 9.56 µm.

3 Results and discussion

A representative temporal temperature profile of the snow sample for both laboratory temperatures of $T_{lab} = -8$ and $-15\,^{\circ}$C is shown in Fig. 2. Variations in temperature up to 1.7 and 1.4 °C were due to heat dissipated by the X-ray tube and temperature fluctuations inside the cold laboratory (Ebner et al., 2014). A longer sintering duration at higher temperature of the snow for experiment "sa3" and "sa4" was used to increase the mean thickness of the ice matrix. This avoided the destruction of the snow structure due to shear stresses caused by the airflow. The structural analysis of the snow samples was conducted on the complete tomography domain (7.2 mm × 7.2 mm × 7.2 mm). A smaller sub-set of 110 × 42 × 110 voxels (2 mm × 0.75 mm × 2 mm) was selected to visualize the 3-D evolution (Fig. 3). It showed no significant change in the grain shape, even for different airflow velocities, and only a slight rounding and coarsening was seen for experiments “sa1” and “sa2”. The residence time of the ice voxels showed disappearance of single ice particles and 13.5 and 9.6 % of the ice matrix for “sa3” and “sa4” (Fig. 4) at the very surface, but the initial ice grains remained. The sublimated mass was relocated to bigger grains but the airflow velocity did not affect this relocation process.

The well-sintered snow showed very little settling under its own weight (Kaempfer and Schneebeli, 2007) and, consequently, no significant change in porosity was observed. This supports the hypothesis that, after sintering, further densification is limited by coarsening kinetics (Kaempfer and Schneebeli, 2007; Schleef et al., 2013). A spatial constant porosity distribution at $t = 0$ days and $t = 4$ days is seen in Fig. 5. Thus, spatial change in the flow field due to different interfacial velocities can be neglected. Consequently, *Pe* was constant with time, and diffusion was still the dominant mass transfer mechanism. The average deviation between $t = 0$ days and $t = 4$ days was 0.5, 1.8, 0.5 and 0.5 % for “sa1”, “sa2”, “sa3” and “sa4”, which was within the range of error of 7.7 % as determined by Zermatten et al. (2014).

Our segmented 3-D data accurately reproduced the original snow sample and the temporal porosity distribution confirmed that no settling and densification occurred (Fig. 6). The gravimetric porosity $\varepsilon_{\text{grav}}$ at the beginning and at the end of each experiment was measured by weighing. The measured density values were converted to porosity ($\varepsilon_{\text{grav}} = 1 - \rho_s/\rho_{\text{ice}}$), and compared to the value of porosity computed by DPLS on the micro-CT geometry. The computed values differed from the measured ones by 1.4 and 0.1 % at the beginning and 4.1 and 2.3 % at the end for experiments “sa3” and “sa4”.

The qualitative progression of the spatial SSA of the scanned snow height for four discs of 7.2 mm × 7.2 mm × 1.8 mm (Fig. 7) did not change significantly with height. This suggested that the snow properties were homogeneous throughout the sample and duration of the experiments. The slight decrease of the spatial SSA for experiment “sa4” is explained by the distribution not initially being completely homogeneous.

The coarsening process led to a decrease of the SSA over time (Fig. 8), which was higher for group "sa1" and "sa2" compared to "sa3" and "sa4". The difference was caused by the 34 % lower initial SSA of group "sa3" and "sa4". Appling the theories developed by Legagneux et al. (2004) and Legagneux and Domine (2005), the evolution of SSA of the ice matrix could be modelled well. The model proposed is given by Legagneux and Domine (2005)

$$\mathrm{SSA} = \mathrm{SSA}_0 \left(\frac{\tau}{\tau + t} \right)^{1/n}, \tag{1}$$

where SSA_0 is the initial SSA at time $t = 0$, n is the growth exponent, and τ a parameter related to grain growth and a form factor. Table 2 shows the fitted parameters and the corresponding normalized root-mean square error (NRMSE) for each experiment. Equation (1) fits the data of each experiment well with an average NRMSE < 0.21. The computed fit of the SSA is shown in Fig. 8. This model is based on the physical processes involved in Ostwald ripening (Ratke and Voorhees, 2002). The driving force in the model is the reduction of the SSA and the model hypothesis is based on the concept that mass transfer occurs by sublimation due to curvature effects, transport through the gas phase and deposition. Theoretically, the growth exponent n is approximately 2 when surface processes are rate limiting and 3 when diffusion is rate limiting. Experiment "sa1" and "sa2" had a higher value of n, indicating a strong coarsening process due to sintering and that surface processes were rate limiting (Legagneux et al., 2004; Legagneux and Domine, 2005). Experiment "sa3" and "sa4" had similar fitting parameters and a lower value of n, suggesting that surface effects were rate limiting. When the sintering times of 13 and 27 days were included in the model, the fitting parameters indicated a consistent growth exponent n for each experiment (Table 3) and a good agreement with the theory. They expressed strong coarsening and surface processes for each experiment. Concluding, the calculated values indicated that surface processes caused the limiting rate rather than the diffusion step and no significant influence of advective transport could be observed.

TCD
9, 1021–1045, 2015

The effect of decreasing SSA on the permeability was not elucidated in our experiments. The effect of increasing airflow velocity had no influence on the flow characteristics (Fig. 9). The value of the effective permeability was higher than the one determined in a previous study (Zermatten et al., 2011, 2014), although, our measured SSA was higher by a factor of at least 2.4. The temporal evolution of permeability for experiment "sa2" showed a decrease of 8 % for the first 40 h and remained constant afterwards. Experiments "sa1", "sa3" and "sa4" showed no significant change in the permeability, which is consistent with the negligible change in density. The average fluctuations of the permeability K between each time step and the slight decrease at the beginning in "sa2" showed small differences that were below the precision of the numerical method with an uncertainty up to 16 % (Zermatten et al., 2014). Only the first time step of "sa3" showed a particularly high difference of 17.3 %, but neither the porosity nor SSA showed significant differences reflecting this value. This difference could therefore be due to an error during the measurement.

No enhanced metamorphism due to the advective process could be observed in any of the experiments. As $Pe < 1$, diffusion was consequently the dominant component. The time scale of diffusion inside the pores ($t_{\mathrm{diff}} = d_{\mathrm{p}}^2/D$) was in the order of 10^{-3} s. The coarsening process can be considered to be independent of mass transfer by advection, which was in the order of 10^{-2} s ($t_{\mathrm{adv}} = d_{\mathrm{p}}/u_{\mathrm{D}}$). Assuming an isothermal snowpack, $Pe > 1$ is unlikely in nature because of: (1) low density snow, which has always a very low strength, will be destroyed due to the high airflow velocity, (2) $Pe > 1$ would be possible for depth hoar, but this snow type is typically found at depth and rarely exposed to high windspeed (Colbeck, 1997b), (3) Pe depends on the temperature due to changing diffusivity. Seasonal temperature fluctuations of −60 to −30 °C are typical for surface snow layer in Antarctic regions, and lead to Pe variations of up to 25 %. Theoretically, $Pe \approx 1.2$ could be realistic at −60 °C for "sa4". However, simulations by Neumann (2003) showed a rapid decrease of the airflow velocity inside the snow layer ($\leq 0.01\,\mathrm{m\,s^{-1}}$) for a high wind speed ($\approx 10\,\mathrm{m\,s^{-1}}$) above the snow surface (pore size ≈ 1 mm). This leads to a maximum $Pe \approx 0.8$ and diffusion is consequently still the dominant driver for snow metamorphism.

4 Summary and conclusions

Four isothermal metamorphism experiments of snow under saturated advective airflow were performed, each with duration of four days. The two main transport processes, diffusion and advection, were analysed inside the pore space. The airflow velocities were chosen based on the Peclet number. $Pe > 0.85$ were not possible due to the destruction of the snow structure. Every 8 h the snow microstructure was observed by X-ray micro-tomography. The micro-CT scans were segmented, and porosity and specific surface area were calculated. Effective permeability was calculated in direct pore-level simulations (DPLS) to analyse the flow characteristic.

The experimental observations supported the hypothesis that, after sintering, further densification was limited by coarsening kinetics and further confirmed a constant porosity evolution (Kaempfer and Schneebeli, 2007). Compared to rates typical for isothermal snow metamorphism, no effect of isothermal advection with saturated air was observed. As predicted by the values of Pe, no enhancement of mass transfer inside the pores was observed and diffusion through the pores was the main driving force. Curvature caused sublimation of small ice grains leading to a slight decrease in SSA. In isothermal snow packs, diffusion through the pores is the dominating part and advective transport processes on the structural dynamics can be neglected.

Acknowledgements. The Swiss National Science Foundation granted financial support under project no. 200020-146540. The authors thank M. Jaggi and S. A. Grimm for technical support with the measurements.

References

Albert, M. R.: Numerical experiments on firn ventilation with heat transfer, Ann. Glaciol., 18, 161–165, 1993.

Albert, M. R. and Mc Gilvary, W. R.: Thermal effects due to air flow and vapour transport in dry snow, J. Glaciol., 38, 274–281, 1992.

Albert, M. R., Shuman, C., Courville, Z., Bauer, R., Fahnestock, M., and Scambos, T.: Extreme firn metamorphism: impact of decades of vapor transport on near-surface firn at a low-accumulation glazed site on the east Antarctic plateau, Ann. Glaciol., 39, 73–78, 2004.

Arnaud, L., Lipenkov, V., Barnola, J., Gay, M., and Duval, P.: Modelling of the densification of polar firn: characterization of the snow-firn transition, Ann. Glaciol., 26, 39–44, 1998.

Bader, H., Haefeli, R., Bucher, E., Neher, J., Eckel, C., and Thams, C.: Der Schnee und seine Metamorphose, Beitr. Geol. Schweiz, Geotechn. Ser.-Hydrol., 3, 1–313, 1939.

Clifton, A., Manes, C., Rüedi, J.-D., Guala, M., and Lehning, M.: On shear-driven ventilation of snow, Bound.-Lay. Meteorol., 126, 249–261, 2008.

Colbeck, S. C.: Thermodynamics of snow metamorphism due to variations in curvature, J. Glaciol., 26, 291–301, 1980.

Colbeck, S. C.: Air movement in snow due to wind-pumping, J. Glaciol., 35, 209–213, 1989.

Colbeck, S. C.: A review of sintering in seasonal snow, Technical Report, 97-10, Cold Regions Research & Engineering Laboratory, Hanover, New Hampshire, 1997a.

Colbeck, S. C.: Model of wind pumping for layered snow, J. Glaciol., 43, 60–65, 1997b.

Colbeck, S. C.: Sintering in a dry snow cover, J. Appl. Phys., 84, 4585–4589, 1998.

Colbeck, S. C.: Sintering of unequal grains, J. Appl. Phys., 89, 4612–4618, 2001.

Cunningham, J. and Waddington, E. D.: Air flow and dry deposition of non-sea salt sulphate in polar firn: paleoclimatic implications, Atmos. Environ., 27A, 2943–2956, 1993.

Domine, F., Albert, M., Huthwelker, T., Jacobi, H.-W., Kokhanovsky, A. A., Lehning, M., Picard, G., and Simpson, W. R.: Snow physics as relevant to snow photochemistry, Atmos. Chem. Phys., 8, 171–208, doi:10.5194/acp-8-171-2008, 2008.

Ebner, P. P., Grimm, A. S., Schneebeli, M., and Steinfeld, A.: An instrumented sample holder for time-lapse micro-tomography measurements of snow under advective conditions, Geosci. Instrum. Methods Data Syst., 3, 179–185, 2014.

Friess, H., Haussener, S., Steinfeld, A., and Petrasch, J.: Tetrahedral mesh generation based on space indicator functions, Int. J. Numer. Meth. Eng., 93, 1040–1056, 2013.

TCD
9, 1021–1045, 2015

Tomography-based monitoring of isothermal snow metamorphism

P. P. Ebner et al.

German, R. M.: Sintering Theory and Practive, John Wiley, New York, 1996.

Gjessing, Y. T.: The filtering effect of snow, in: Isotopes and Impurities in Snow and Ice Symposium, edited by: Oeschger, H., Ambach, W., Junge, C. E., Lorius, C., and Serebryanny, L., 118, IASH-AISH Publication, Dorking, 199–203, 1977.

Grannas, A. M., Jones, A. E., Dibb, J., Ammann, M., Anastasio, C., Beine, H. J., Bergin, M., Bottenheim, J., Boxe, C. S., Carver, G., Chen, G., Crawford, J. H., Dominé, F., Frey, M. M., Guzmán, M. I., Heard, D. E., Helmig, D., Hoffmann, M. R., Honrath, R. E., Huey, L. G., Hutterli, M., Jacobi, H. W., Klán, P., Lefer, B., McConnell, J., Plane, J., Sander, R., Savarino, J., Shepson, P. B., Simpson, W. R., Sodeau, J. R., von Glasow, R., Weller, R., Wolff, E. W., and Zhu, T.: An overview of snow photochemistry: evidence, mechanisms and impacts, Atmos. Chem. Phys., 7, 4329–4373, doi:10.5194/acp-7-4329-2007, 2007.

Hobbs, P. V. and Mason, B. J.: The sintering and adhesion of ice, Philos. Mag., 9, 181–197, 1963.

Kaempfer, T. U. and Schneebeli, M.: Observation of isothermal metamorphism of new snow and interpretation as a sintering process, J. Geophys. Res., 112, 1–10, 2007.

Kingery, W. D.: On the metamorphism of snow, in: International Geological Congress, XXI Sesion, Norden, Copenhagen, 15–25 August 1960, 81–89, 1960a.

Kingery, W. D.: Regelation, surface diffusion, and ice sintering, J. Appl. Phys., 31, 833–838, 1960b.

Kuroiwa, D.: A study of ice sintering, Tellus, 13, 252–259, 1961.

Legagneux, L. and Domine, F.: A mean field model of the decrease of the specific surface area of dry snow during isothermal metamorphism, J. Geophys. Res., 110, F04011, doi:10.1029/2004JF000181, 2005.

Legagneux, L., Taillandier, A. S., and Domine, F.: Grain growth theories and the isothermal evolution of the specific surface area of snow, J. Appl. Phys., 95, 6175–6184, 2004.

Legrand, M. and Mayewski, P.: Glaciochemistry of polar ice cores: a review, Rev. Geophys., 35, 219–243, 1997.

Löwe, H., Spiegel, J. K., and Schneebeli, M.: Interfacial and structural relaxations of snow under isothermal conditions, J. Glaciol., 57, 499–510, 2011.

McConnell, J. R., Bales, R. C., Stewart, R. W., Thompson, A. M., Albert, M. R., and Ramos, R.: Physically based modelling of atmosphere-to-snow-to-firn transfer of H_2O_2 at the South Pole, J. Geophys. Res., 103, 10561–10570, 1998.

Maeno, N. and Ebinuma, T.: Pressure sintering of ice and its implication to the densification of snow at polar glaciers and ice sheets, J. Phys. Chem.-US, 87, 4103–4110, 1983.
Neumann, T. A.: Effects of Firn Ventilation on Geochemistry of Polar Snow, Ph.D. thesis, University of Washington, Washington, 2003.
Neumann, T. A. and Waddington, E. D.: Effects of firn ventilation on isotopic exchange, J. Glaciol., 50, 183–194, 2004.
Neumann, T. A., Albert, M. R., Engel, C., Courville, Z., and Perron, F.: Sublimation rate and the mass transfer coefficient for snow sublimation, Int. J. Heat Mass. Tran., 52, 309–315, 2009.
Otsu, N.: A threshold selection method from gray-level histograms, IEEE T. Syst. Man. Cyb., 9, 62–66, 1979.
Pinzer, B. R. and Schneebeli, M.: Breeding snow: an instrumented sample holder for simultaneous tomographic and thermal studies, Meas. Sci. Technol., 20, 1–9, 2009.
Pinzer, B. R., Schneebeli, M., and Kaempfer, T. U.: Vapor flux and recrystallization during dry snow metamorphism under a steady temperature gradient as observed by time-lapse microtomography, The Cryosphere, 6, 1141–1155, doi:10.5194/tc-6-1141-2012, 2012.
Ratke, L. and Voorhees, P. W.: Growth and Coarsening, Springer, Berlin, Heidelberg, Germany, ISBN 978-3-540-42563-2, 2002.
Schleef, S. and Löwe, H.: X-ray microtomography analysis of isothermal densification of new snow under external mechanical stress, J. Glaciol., 59, 233–243, 2013.
Schleef, S., Jaggi, M., Löwe, H., and Schneebeli, M.: Instruments and methods: an improved machine to produce nature-identical snow in the laboratory, J. Glaciol., 60, 94–102, 2014.
Schneebeli, M. and Sokratov, S.: Tomography of temperature gradient metamorphism of snow and associated changes in heat conductivity, Hydrol. Process., 3665, 3655–3665, 2004.
Severinghaus, J. P., Albert, M. R., Courville, Z. R., Fahnestock, M. A., Kawamura, K., Montzka, S. A., Muehle, J., Scambos, T. A., Shields, E., Shuman, C. A., Suwa, M., Tans, P., and Weiss, R. F.: Deep air convection in the firn at a zero-accumulation site, central Antarctica, Earth Planet. Sc. Lett., 293, 359–367, 2010.
Sowers, T., Bender, M., Raynard, D., and Korotkevich, Y. S.: δ^{15}N in air trapped in polar ice: a tracer of gas transport in the firn and a possible constraint on ice age-gas age differences, J. Geophys. Res., 97, 15683–15697, 1992.
Stössel, F., Guala, M., Fierz, C., Manes, C., and Lehning, M.: Micrometeorological and morphological observations of surface hoar dynamics on a mountain snow cover, Water Resour. Res., 46, 1–11, 2010.

Sturm, M. and Johnson, J. B.: Natural convection in the subarctic snow cover, J. Geophys. Res., 96, 11657–11671, 1991.
Vetter, R., Sigg, S., Singer, H. M., Kadau, D., Herrmann, H. J., and Schneebeli, M.: Simulating isothermal aging of snow, Europhys. Lett., 89, 26001, doi:10.1209/0295-5075/89/26001, 2010.
Waddington, E. D., Cunningham, J., and Harder, S. L.: The effects of snow ventilation on chemical concentrations, in: Chemical Exchange Between the Atmosphere and Polar Snow, edited by: Wolff, E. W. and Bales, R. C., NATO ASI Series, 43, Springer, Berlin, 403–452, 1996.
Zermatten, E., Haussener, S., Schneebeli, M., and Steinfeld, A.: Instruments and Methods: tomography-based determination of permeability and Dupuit–Forchheimer coefficient of characteristic snow samples, J. Glaciol., 57, 811–816, 2011.
Zermatten, E., Schneebeli, M., Arakawa, H., and Steinfeld, A.: Tomography-based determination of porosity, specific area and permeability of snow and comparison with measurements, Cold Reg. Sci. Technol., 97, 33–40, 2014.

Table 1. Morphological and flow characteristics of the experiments: volume flow ($\dot{V}$), corresponding Peclet number (*Pe*), Reynolds number (*Re*), initial superficial velocity in snow ($u_{D,0}$), initial snow density (ρ_0) (±7.7 %), initial porosity (ε_0) (±7.7 %), specific surface area (SSA_0) (±18.8 %), initial pore diameter (d_p), temperature in the cold laboratory (T_{lab}), and the sintering time of the snow.

Name	$\dot{V}$ L min^{-1}	*Pe*	*Re*	$u_{D,0}$ m s^{-1}	ρ_0 kg m^{-3}	ε_0	SSA_0 m^2 kg^{-1}	d_p mm	T_{lab} °C	Sintering time
sa1	–	–	–	–	226.43	0.75	46.6	0.22	−8.0	13 days at −15 °C
sa2	0.36	0.05	0.07	0.004	186.1	0.78	43.7	0.27	−8.0	13 days at −15 °C
sa3	3.0	0.47	0.6	0.04	325.43	0.65	28.7	0.24	−15.0	27 days at −5 °C
sa4	5.0	0.85	1.1	0.06	264.93	0.71	28.0	0.29	−15.0	27 days at −5 °C

TCD
9, 1021–1045, 2015

Table 2. Values of the fitted growth rate τ and growth exponent n for the evolution of the SSA and the corresponding normalized root-mean square error (NRMSE).

Name	SSA_0 $m^2\,kg^{-1}$	τ	n	NRMSE
sa1	46.7	632.9	2.10	0.01
sa2	43.6	721.2	2.15	0.04
sa3	27.8	14 400	0.32	0.14
sa4	27.8	17 380	0.39	0.21

TCD
9, 1021–1045, 2015

Tomography-based monitoring of isothermal snow metamorphism

P. P. Ebner et al.

Table 3. Values of the fitted growth rate τ and growth exponent n for the evolution of the SSA including the sintering time of 13 and 27 days, and the corresponding normalized root-mean square error (NRMSE).

Name	SSA_0 $m^2\,kg^{-1}$	τ	n	NRMSE
sa1	64.4	320.9	2.10	0.01
sa2	56.8	409.1	2.15	0.04
sa3	34.5	1229	2.0	0.15
sa4	36.0	1063	1.91	0.27

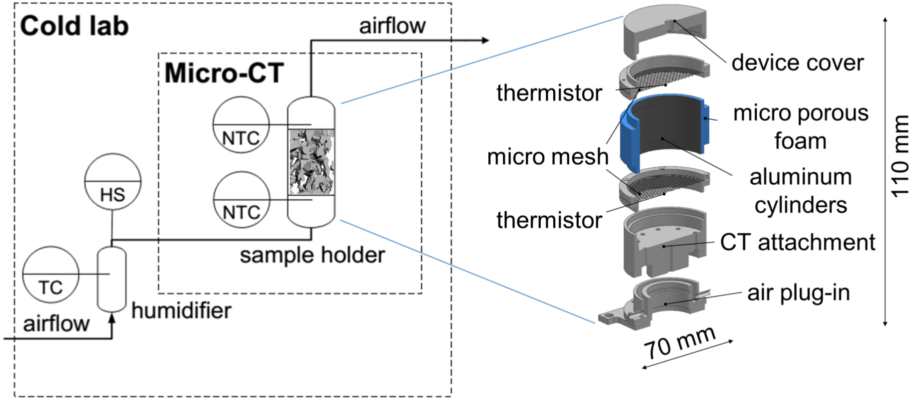

Figure 1. Schematic of the experimental setup and the sample holder. A thermocouple (TC) and a humidifier sensor (HS) inside the humidifier measured the airflow conditions. Two thermistors (NTC) close to the snow surface measured the inlet and outlet temperature of the airflow (Ebner et al., 2014).

TCD
9, 1021–1045, 2015

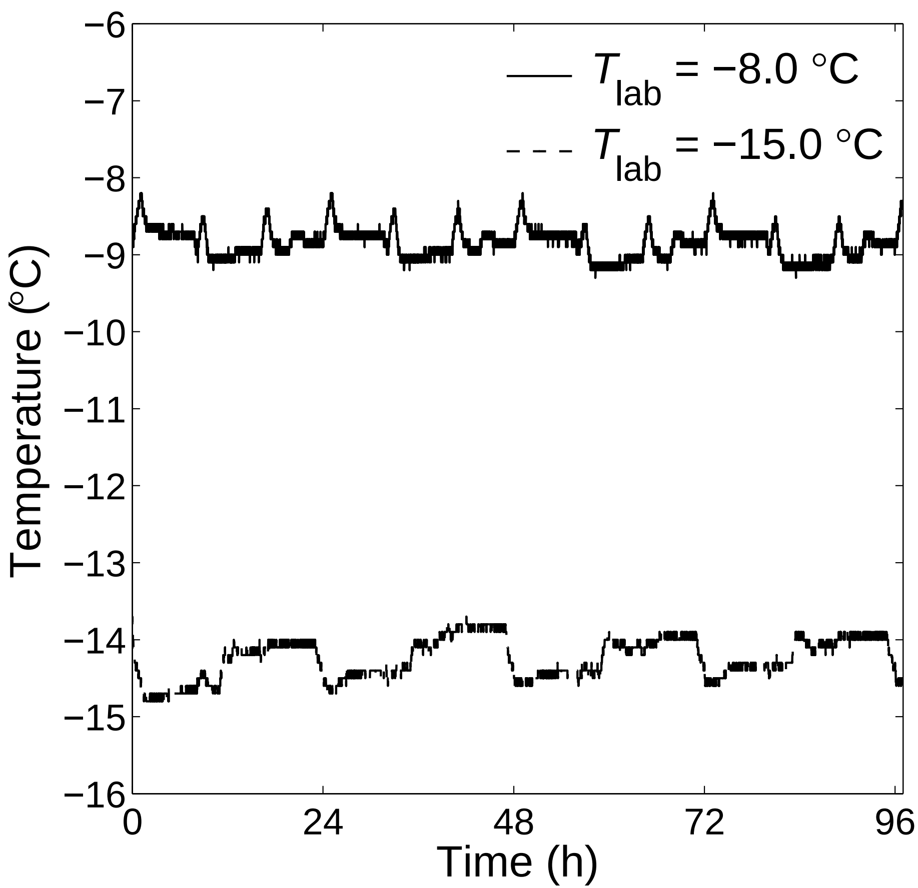

Figure 2. A typical temperature profile for experiment "sa1, sa2" and "sa3, sa4". The temperature rise was caused by the X-ray tube and fluctuations inside the cold laboratory (Ebner et al., 2014).

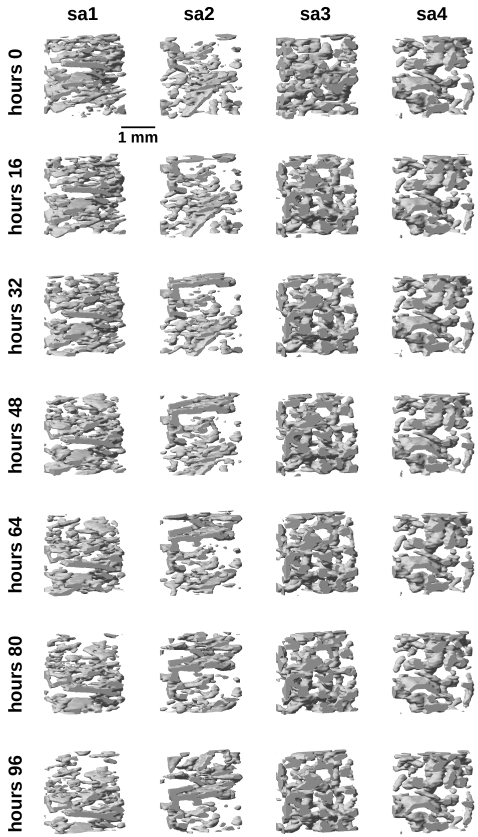

Figure 3. Evolution of the 3-D structure of the ice matrix during isothermal metamorphism under advective conditions. Experimental conditions (from left to right) at different measurement times from beginning to the end (top to bottom) of the experiment. The shown cubes are 110 × 42 × 110 voxels (2 mm × 0.75 mm × 2 mm) large.

TCD
9, 1021–1045, 2015

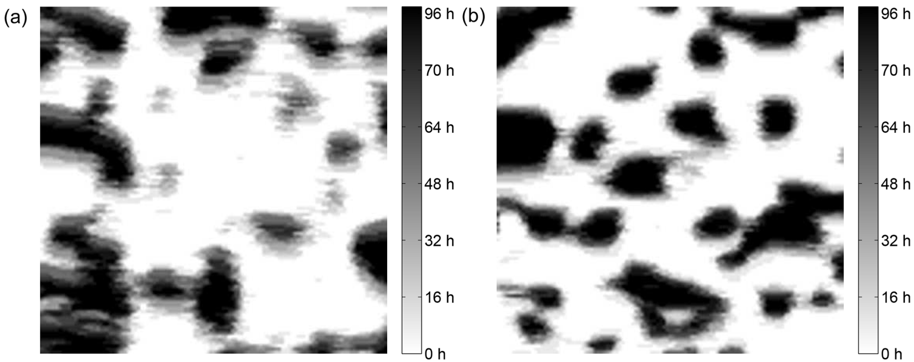

Figure 4. Residence time of ice particles within in a slice (5.7 mm × 5.7 mm) parallel to the flow direction for **(a)** “sa3” and **(b)** “sa4” by overlapping time-lapse tomography pictures. The period of 8 h was sufficiently short to calculate the residence time of each ice voxel with an uncertainty of 6 %.

TCD
9, 1021–1045, 2015

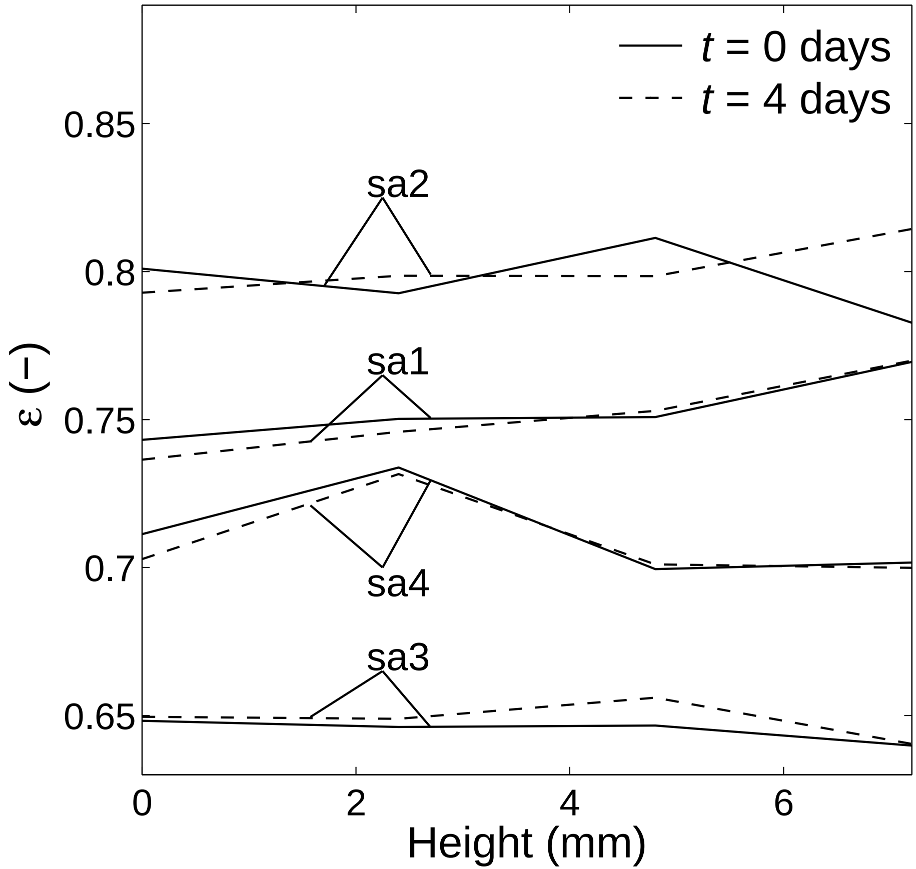

Figure 5. Spatial porosity profile of the scanned area at the beginning and at the end of each experiment with an uncertainty of 7.7 % (Zermatten et al., 2014). The spatial variability within the reconstructed volume was measured in four discs of 7.2 mm × 7.2 mm × 1.8 mm.

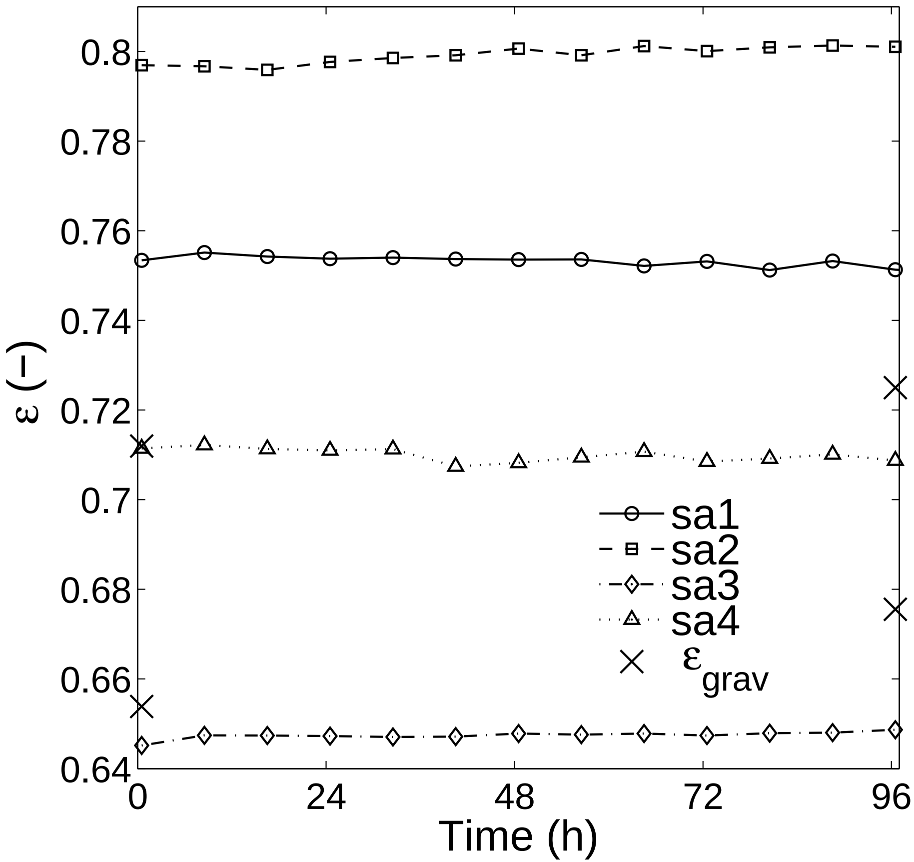

Figure 6. Evolution of the porosity over time obtained by triangulated structure surface method with an uncertainty of 7.7 % (Zermatten et al., 2014) and the measured gravimetric density ($\varepsilon_{\text{grav}}$) at the beginning and at the end of "sa3" and "sa4".

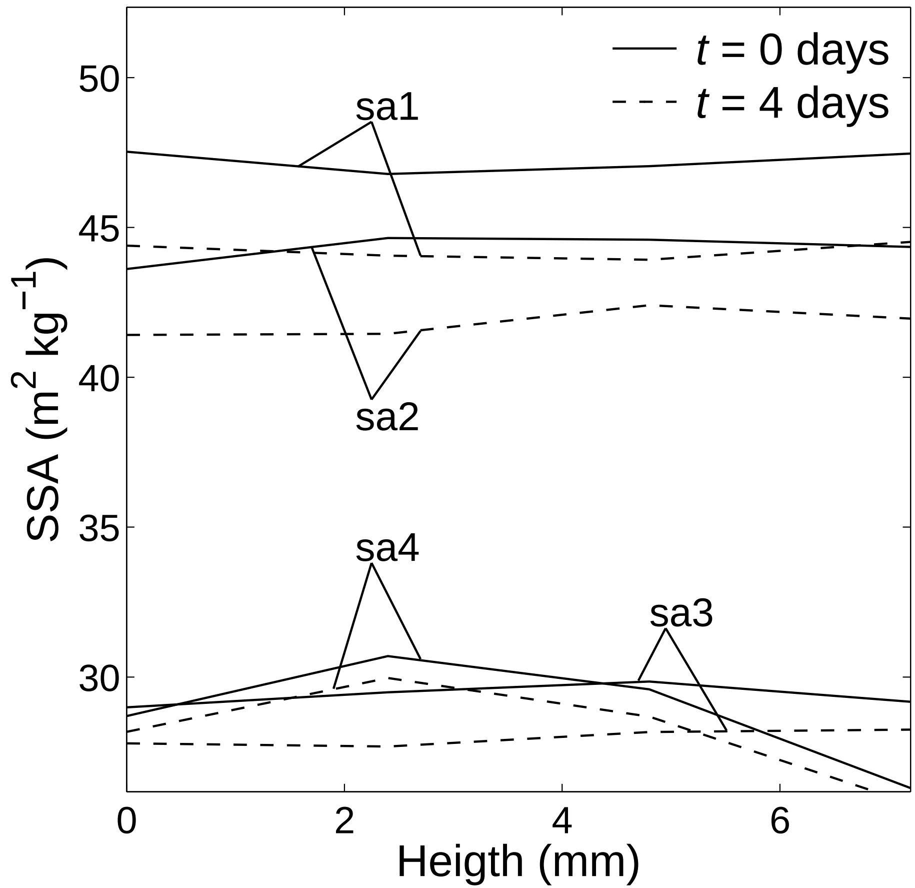

Figure 7. Spatial SSA profile of the scanned area at the beginning and at the end of each experiment with an uncertainty of 18.8 % (Zermatten et al., 2014). The spatial variability within the reconstructed volume was measured in four discs of 7.2 mm × 7.2 mm × 1.8 mm.

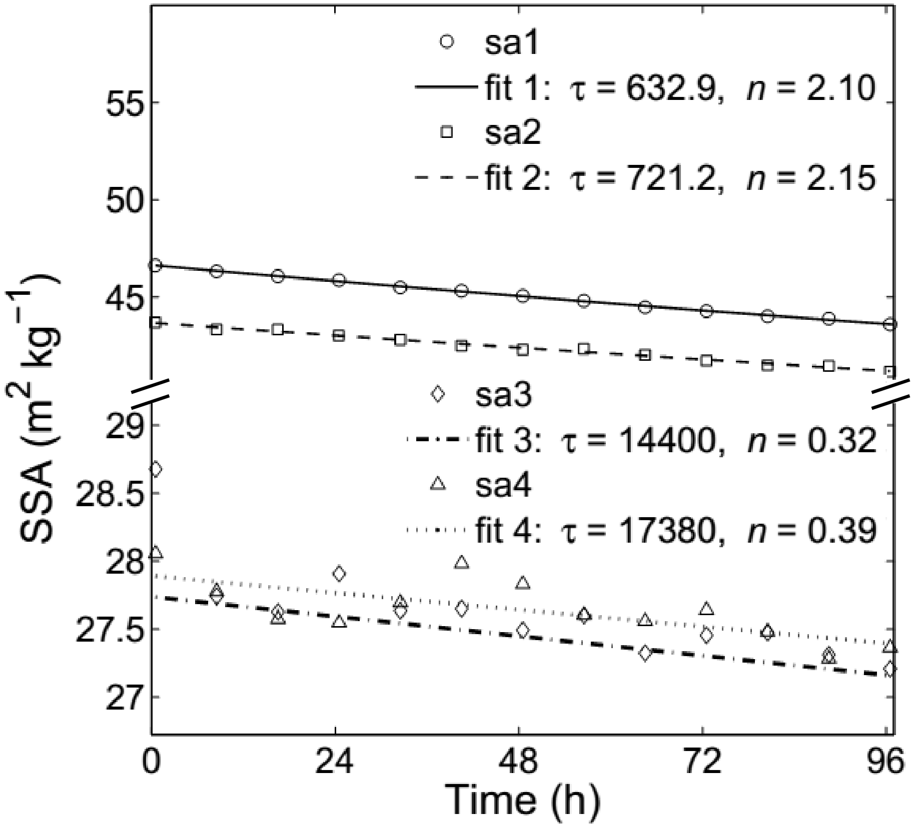

Figure 8. Temporal evolution of the specific surface area, SSA, of the ice matrix obtained by triangulated structure surface method with an uncertainty of 18.8 % (Zermatten et al., 2014). The computed fit is of the form $\mathrm{SSA}(t) = \mathrm{SSA}_0 \left(\frac{\tau}{\tau + t}\right)^{1/n}$.

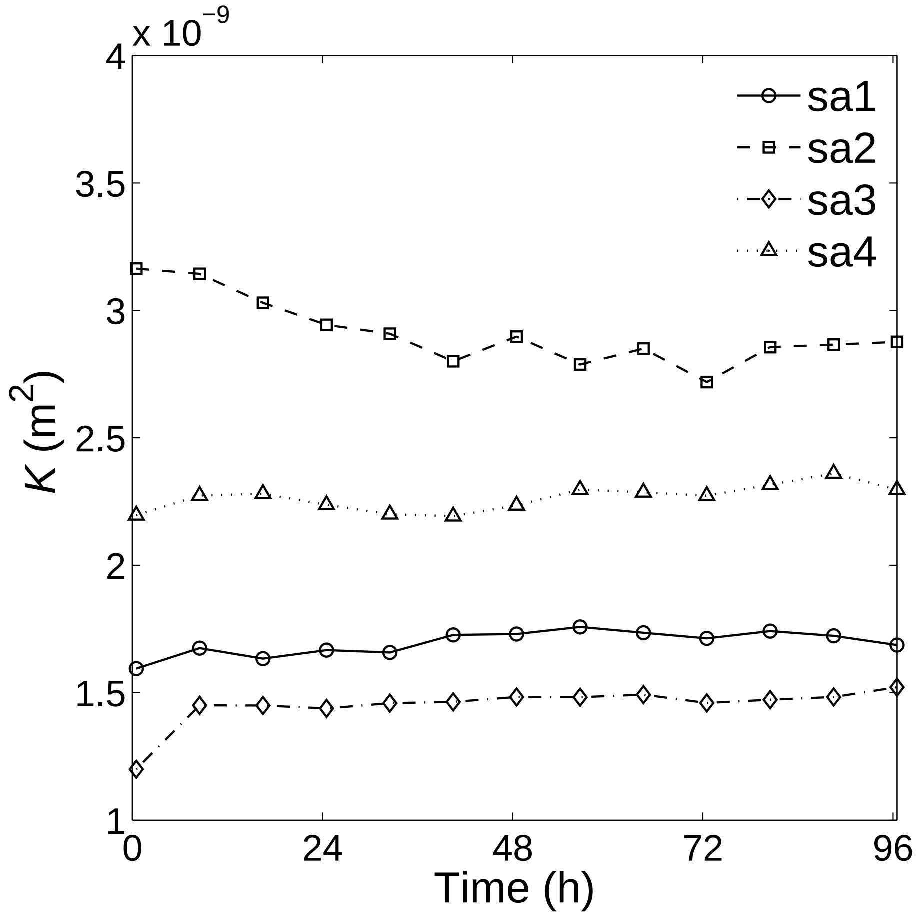

Figure 9. Temporal evolution of the effective permeability by applying DPLS with an uncertainty of 16 % (Zermatten et al., 2014).

TCD
9, 1021–1045, 2015